OUTSTANDING SYMPOSIUM PAPERS

Articles in this section are based on presentations that were selected by MRS Meeting Symposium Organizers as outstanding papers. Upon selection, authors are invited to submit their research results to Journal of Materials Research. *These papers are subject to the same peer review and editorial standards as all other JMR papers. This is another way by which the Materials Research Society recognizes high quality papers presented at its meetings.*

Effect of mobile cation on zeolite-polyamide thin film nanocomposite membranes

Mary Laura Lind, Byeong-Heon Jeong,[a] Arun Subramani,[b] Xiaofei Huang, and Eric M.V. Hoek[c]
UCLA Civil & Environmental Engineering Department, and California NanoSystems Institute, University of California—Los Angeles, Los Angeles, California 90095

(Received 20 August 2008; accepted 2 December 2008)

Hybrid zeolite-polyamide thin film nanocomposite (TFN) reverse osmosis membranes were synthesized by incorporating Linde type A (LTA)-type zeolite molecular sieve nanocrystals in the interfacial polymerization reaction used to form polyamide thin films. Nanocrystals were prepared with two different mobile cations (Na^+ and Ag^+) exchanged within the LTA crystal matrix. Incorporation of molecular sieve nanocrystals into polyamide thin films during interfacial polymerization was verified by infrared spectroscopy. Both TFN membranes exhibited higher water permeability, while maintaining similar salt rejection to pure polyamide thin film composite membranes. Nanocomposite thin films containing LTA nanocrystals in the silver form (AgA) produced a greater increase in water permeability than those in the sodium form (NaA). Furthermore, AgA-TFN membranes exhibited more hydrophilic and smooth interfaces, which appeared to inhibit adhesion of bacteria cells onto the membranes. The AgA nanocrystals exhibited significant bactericidal activity; however, when encapsulated within polyamide thin films the antimicrobial activity was significantly reduced.

I. INTRODUCTION

Water is fundamental for human survival and is a critical limiting resource powering the global economy through its use in agricultural irrigation, electricity production, and industrial processes. As demand approaches the amount of fresh water available, purification of nontraditional water from sources will be critical.[1] Reverse osmosis (RO) membranes are now among the most popular technologies for producing fresh water from alternative waters—such as seawater, brackish groundwater, and wastewater—because commercially available RO membranes can produce high-quality water from virtually any source. However, RO membranes with higher water permeability, improved contaminant selectivity, and better fouling resistance are needed to reduce the operating costs, chemical consumption, and energy demand of producing high-quality water from alternative sources.

Nanotechnology promises to provide entirely new classes of functional materials for application to water purification—including better filter media, sorbents, catalysts, and membranes.[2] Promising examples of advanced nanotechnology-based membranes include those based on aligned carbon nanotubes, hybrid protein-polymer biomimetic membranes, and thin film nanocomposite membranes.[3] Each of these approaches to fabricating advanced water purification membranes is exciting and worthy of continued research to better understand the fundamental principles underlying membrane formation, material properties, and separation performance. Inorganic–organic nanocomposite membranes are particularly interesting because they exhibit enhanced water permeability, good solute rejections, and improved interfacial properties, including antimicrobial and photocatalytic reactivity.[4,5]

Herein we present new results from hand casting and laboratory testing of thin film nanocomposite RO membranes formed by interfacial polymerization. Specifically, we report on the separation performance, interfacial properties, and fouling resistance of zeolite-polyamide nanocomposite thin films formed with sodium and silver cations exchanged within zeolite molecular sieve nanocrystals. The morphology and structure of thin films provided new insights into the potential role that zeolite nanocrystals play in thin film polymerization,

[a]Present address: Hyundai & Kia Motors, 104 Mabuk-Dong, Giheung-Gu, Yongin-Si, Gyeonggi-Do 446-912, Korea.
[b]Present address: MWH, 618 Michillinda Avenue, Suite 200, Arcadia, CA 91007.
[c]Address all correspondence to this author.
e-mail: hoek@seas.ucla.edu

This paper was selected as an Outstanding Symposium Paper for the 2007 MRS Fall Meeting, Symposium V.
DOI: 10.1557/JMR.2009.0189

and ultimately, on the observed separation performance, interfacial properties, and fouling resistance of the membranes. Implications of these advanced materials are discussed with respect to the need for improved RO membranes in desalination and water purification.

II. EXPERIMENTAL

As previously reported by Jeong et al.,[5] nanocrystals of Linde type A (LTA) zeolites were synthesized in the sodium form (NaA) by a hydrothermal method. The crystalline structure of as-synthesized LTA nanocrystals was confirmed by x-ray diffraction.[5] Average zeolite particle size and polydispersity were evaluated by scanning electron microscopy (SEM) and dynamic light scattering (DLS) and was found to range from ~50 to ~250 nm with mean hydrodynamic diameter of 140 nm.[5]

In this study, we consider identically fabricated LTA particles with two different mobile cations: as-synthesized NaA nanocrystals and LTA nanocrystals with silver ions exchanged for sodium ions (AgA). All aqueous solutions were prepared with 18 MΩ distilled and deionized laboratory water. As-synthesized NaA nanocrystals were dispersed at 0.1% w/w in 0.1 M aqueous $AgNO_3$ solution. The dispersion was stirred for 12–15 h at room temperature, and the solution was then centrifuged and the particles washed with deionized water three times, thus creating AgA nanocrystals.

Energy dispersive x-ray spectroscopy (EDX) (Genesis Spectrum EDAX, Ametek, Paoli, PA) analysis of the LTA nanocrystals was performed to determine elemental content as well as the success and extent of silver cation exchange. The LTA nanocrystals were suspended in water and then a drop was placed on the conducting stub with carbon tape. The water was allowed to evaporate from the stub overnight at room temperature in a closed desiccator before SEM imaging (Hitachi S-4700, Schaumburg, IL) and EDX analysis.

Pure polyamide and zeolite-polyamide nanocomposite thin films were hand cast on commercially fabricated porous polysulfone (PSf) ultrafiltration membranes (Sepro, Oceanside, CA) as follows. A PSf membrane was immersed for 15 s in a solution of 2.3:6.6:0.02% (w/v) aqueous solution of *m*-phenylenediamine (MPD, >99%; Sigma-Aldrich, St. Louis, MO), the salt of triethylamine (TEA, liquid, 99.5%; Sigma-Aldrich) and (+)-10-champhor sulfonic acid (CSA, powder, 99.0%; Sigma-Aldrich), and sodium lauryl sulfate (SLS; Sigma-Aldrich). The MPD: TEA-CSA:SLS mixture was produced as previously described by Ghosh et al.[6] Excess aqueous monomer solution was removed from the membrane using a custom fabricated air knife. The PSf membrane was then immersed in a solution of 0.1% (w/v) trimesoyl chloride (TMC, 98%; Sigma-Aldrich) in a commercial isoparaffin (Isopar-G; Gallade Chemicals, Santa Ana, CA) hereafter referred to as "isopar." After 1 min of reaction, the TMC solution was poured off and the membranes were rinsed with an aqueous solution of 0.2% (w/v) sodium carbonate [high-performance liquid chromatography (HPLC)-grade; Fisher Scientific, Pittsburgh, PA].

Nanocomposite thin films were hand cast identically after dispersing 0.4% (w/v) of zeolite nanocrystals in the isopar-TMC solution by ultrasonication for 1 h; maintaining a sonication bath temperature of 20 °C by periodic addition of ice. The dispersion was used for the interfacial polymerization reaction immediately after sonication.

Thin film morphology was imaged by SEM at an accelerating voltage of 10 kV and a working distance of 10 mm. Dried membrane samples were mounted on a conducting sample holder with double-sided carbon tape and then sputter coated with an ~20-nm-thick layer of Au-Pd. Surface roughness of the synthesized membranes was quantified with an atomic force microscope (AFM; Nanoscope IIIa, Digital Instruments, Plainview, NY). A silicon nitride cantilever tip (NSC 14; MikroMasch, San Jose, CA) was used at a fixed scanning rate of 1 Hz. The tip radius was less than 10 nm, and the cantilever length was 125 μm with a spring constant of 5 N/m. Membrane surfaces were scanned dry in air using the "tapping mode," which is appropriate for soft polymers.[7]

Thin film functionality was assessed by Fourier transform infrared spectroscopy (FT/IR 670 plus; Jasco, Easton, MD), and performed with a variable angle attenuated total reflection (ATR) attachment coupled to a germanium crystal operated at 45 degrees. Prior to ATR-IR measurement, the samples were dried in a desiccator for a minimum of 24 h. Surface (zeta) potential of hand-cast membranes was determined by measuring the streaming potential (BI-EKA, Brookhaven Instrument Corp., Holtsville, NY) with 10 mM NaCl solution at unadjusted pH (5.8 ± 0.2).

Separation performance of the membranes was evaluated using deionized water and 2000 ppm NaCl or polyethylene glycol (PEG) aqueous solutions. The PEG had a molecular weight of 200 Da according to the supplier (P3015; Sigma-Aldrich). Hand-cast membranes were mounted in a high-pressure chemical resistant stirred cell (HP4750 Stirred Cell, Sterlitech Corp., Kent, WA) with an effective membrane area of 13.85 cm^2. Pure water flux was measured at room temperature (20 °C) after the membranes were compressed for 3 h at 1.55 MPa. Solute rejection was obtained from the average of initial and final feed concentrations and the average permeate concentration at a permeate recovery of 50%. Four coupons from each membrane were evaluated to determine average water permeability and solute rejections.

Bacterial deposition experiments were performed using a microscopic observation and image analysis technique that has been described in detail elsewhere.[8–10] Briefly, hand-cast thin film composite (TFC) and thin

film nanocomposite (TFN) membranes were placed in a cross-flow membrane filtration module with the active surface of the membrane facing up. The top plate of the membrane module contains a glass window through which one can view the membrane surface using a standard upright fluorescent microscope outfitted with green and red filters (BX51WI, Olympus, Center Valley, PA).

The membrane module and flow system were designed to permit real-time, direct visual observation of the rate of bacterial deposition onto membranes. The module can withstand internal hydraulic pressures up to 300 psi making it possible to simulate practical RO operating conditions for salinities up to about ~100 mM, which covers the salinity range of fresh water, wastewater, and most brackish waters. The module is mounted on the microscope stage and a series of pumps, valves, pressure gages, and flow gages enable accurate control of hydrodynamic conditions in the module.

The system pressure and flow were set to produce a cross-flow Reynolds number of 250, but no permeation through the membrane. We have previously observed the rate of Brownian deposition of bacteria cells (i.e., with no water permeation through the membrane) onto RO membranes correlates strongly with membrane surface properties (hydrophilicity, roughness, charge, etc.) and is indicative of the short-term fouling resistance of a membrane.[9] The fractional surface coverage of bacteria on the membrane was quantified periodically over a total duration of 40 min to produce the fractional surface coverage of cells deposited on the membranes.

A gram-negative aerobic bacterium, *Pseudomonas putida*, was used as a model microorganism to study microbial adhesion and inactivation by the membranes and nanocrystals. The pure bacterial culture cells were cultured in trypticase soy broth (TSB; Difco, Detroit, MI); suspended and grown at 25°, shaken at 150 rpm, and incubated until the exponential phase was reached, at which time cells were harvested by centrifugation at 3800 *g*.[9] The nutrient solution used throughout this study was TSB; the rinse solution was a standard phosphate buffer solution (PBS). The medium was prepared by dissolving 30 g of TSB powder into 1 L of deionized water. The nutrient solution had a pH of ~6.0 and a conductivity of ~11 mS/cm. The PBS was prepared by dissolving 0.2 g KCl, 0.2 g KH_2PO_4, 8 g NaCl, 0.1 g $MgCl_2{\cdot}6H_2O$, 1.15 g $Na_2HPO_4{\cdot}2H_2O$, and 0.1 g $CaCl_2$ in 1.0 l of deionized water.[11] Bacterial suspensions were prepared for deposition experiments by dispersing 10^6 to 10^7 cells·mL^{-1} in solutions of 10 mM NaCl at unadjusted pH (5.8 ± 0.2) and constant temperature of 20 ± 2 °C.

After deposition experiments, the viability of bacteria deposited onto TFC and TFN membranes was determined using a commercially available differential florescent stain kit (Live/Dead BaclightL13152, Molecular Probes Invitrogen, Carlsbad, CA). Mixtures in the ratio 2:1 of SYTO 9 (green fluorescent nucleic acid stain) and propidium iodide (red fluorescent stain) were applied directly to membrane samples after filtering a bacteria suspension. In addition, viability of cells in the bulk suspensions was verified by adding the stains to 1 mL of the bacterial cell suspension. The stained membranes or cell suspensions were stored in the absence of light for 15 min after which the cells were analyzed by differential fluorescence microscopy (BX51WI; Olympus). Two different filters, a red and a green, were used to observe the dead and live cells, respectively.

III. RESULTS

The EDX spectra presented in Fig. 1 verify that the NaA and AgA zeolite nanocrystals contain predominantly Na^+ and Ag^+ cations, respectively. Quantitative analysis of EDX data suggest that greater than 90% of the Na^+ was replaced by Ag^+ in the exchange process. Li et al.[12] measured the pore sizes of bulk LTA crystals using nitrogen porosimetry. They suggested that NaA has a pore size of 4.2 Å, whereas AgA has a pore size of 3.5 Å.

Photographs of TFC and TFN membranes just after synthesis are presented in Fig. 2. The TFN membrane containing AgA nanocrystals exhibits a distinctly different surface color from the other two types of membranes. The purple-brown color indicates precipitation of an insoluble silver species (e.g., silver chloride or metallic silver) on or within the thin film. Apparently, silver ions were displaced from the zeolite crystals during the interfacial polymerization reaction and replaced with another charge neutralizing cation—probably sodium or hydrogen ions, which are both present at significant concentrations in the aqueous monomer solution. Hydrogen and chloride ions are produced as MPD reacts with TMC, while sodium is the anionic surfactant

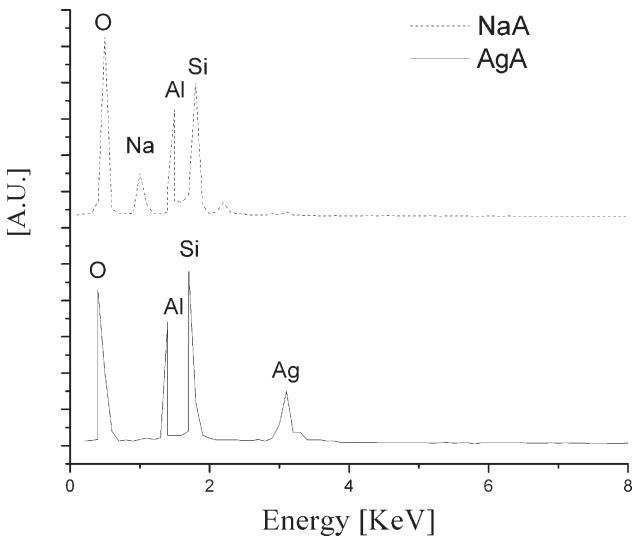

FIG. 1. EDX spectra of NaA and AgA nanocrystals.

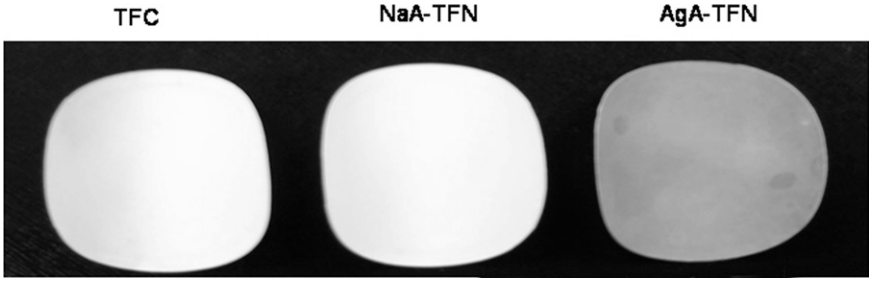

FIG. 2. Photographic images characteristic of as-cast TFC, NaA-TFN, and AgA-TFN membranes.

counter-ion. The color of AgA-TFN membranes did not fade after filtering deionized water or NaCl and PEG solutions. Furthermore, membranes stored in deionized water at 5 °C retained this purple-brown color for over one year before they were disposed, which suggests the silver precipitate is stable for long periods in water.

Figure 3(a) shows pure water flux and solute rejection for TFC, NaA-TFN, and AgA-TFN membranes. Both TFN membranes exhibit higher water permeability than the TFC membrane. The AgA-TFN membranes have significantly higher pure water flux than NaA-TFN membranes, while maintaining similar rejections of both NaCl and PEG. For perspective, when similarly tested, commercially fabricated seawater, brackish water, and high flux RO membranes produced pure water permeabilities of 2.6 ± 0.3, 16.8 ± 0.8, and 27.7 ± 1.7 μm·$MPa^{-1}s^{-1}$ and NaCl rejections of 92.0 ± 1.9, 93.0 ± 1.2, and 75.2 ± 3.1%.[5] Because the characteristic pore dimension of AgA nanocrystals (~3.5 Å) is smaller than that of NaA nanocrystals, the permeability of AgA-TFN membranes was expected to be smaller. However, there was evidence of silver being released from the nanoparticles during the interfacial polymerization reaction (i.e., the purple-brown color), possibly replaced by sodium ions, hydrogen ions, or some mixture of sodium and hydrogen ions.

Previously, Jeong et al.[5] demonstrated the permeability of pore-open and pore-filled NaA-TFN membranes were different, but both larger than pure polyamide TFC membranes. Pore-open NaA-TFN membranes exhibited the highest permeability followed by pore-filled NaA-TFN and TFC membranes, respectively. These results supported the importance of zeolite pore structure for producing high-flux TFN membranes. However, because pore-filled nanoparticles also produced higher flux, it was speculated that zeolite nanocrystals present during the interfacial polymerization reaction could alter the bulk or local polyamide film structure through another mechanism. In this study, the silver released from AgA zeolites during the interfacial polymerization could have altered interfacial polymerization kinetics, possibly by scavenging chloride ions and producing a slightly more permeable polymer film structure.[6]

In Fig. 3(b), average surface roughness (R_a), surface area difference (SAD), and zeta potential of hand-cast

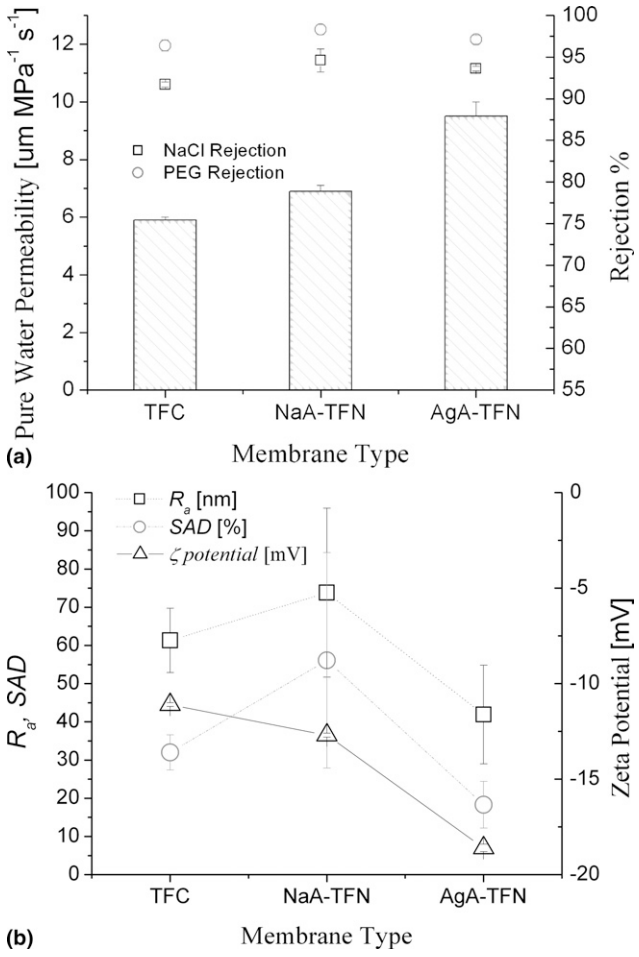

FIG. 3. Characteristic (a) separation performance and (b) interfacial properties of TFC and TFN membranes.

TFC and TFN membranes are presented. Each of these properties changed significantly with the addition of zeolites to the polyamide film. The AgA membrane has a significantly lower surface area and average roughness, as well as a more negative zeta potential. Although contact angles were not obtained for these membrane samples, polyamide membranes exhibit a strong correlation between zeta potential and hydrophilicity (i.e., polarity), where increasingly negative zeta potential is associated with a more hydrophilic interface.[5] Generally, colloidal

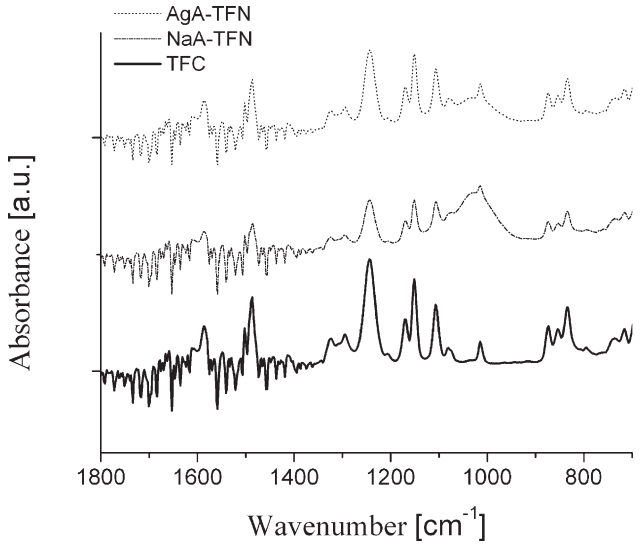

FIG. 4. ATR-IR spectra for TFC and TFN membranes.

and bacterial fouling are reduced as RO membrane interfaces become more smooth, negatively charged, and hydrophilic.[9,13]

Figure 4 shows the ATR-IR spectra for the base TFC membrane and both TFN membranes. The base TFC membrane has the spectrum expected for a polyamide-polysulfone thin film composite.[14,15] The sharp peaks seen in the TFC membrane at 1014 and 1081 cm^{-1} are due to the polysulfone backing material. Membranes made with NaA and AgA nanocrystals have nearly identical spectra to the TFC membrane except for the broad background peak in the "fingerprint region" from ~1100–950 cm^{-1}, thus this broad background peak appears to be attributable to the presence of LTA nanocrystals. The broad background peak for both TFN membranes appears to be attributed to SiO–M (M = Na, K, Ag, etc.) between 1000 and 900 cm^{-1}, or essentially the presence of LTA nanocrystals.[16–18] This peak amplitude is larger for the NaA-TFN membrane than it is for the AgA-TFN membrane; suggesting that more NaA was incorporated than AgA in the TFN films. The FTIR spectra confirm that nanocrystals are present in or on the polyamide films; however, the exact nature of interaction between the zeolite and polymer is not elucidated.

In Fig. 5, representative SEM images are presented for the three hand-cast membranes. These images were obtained specifically for small regions of the polymer appearing to contain no nanocrystals to elucidate differences in the morphology of the polyamide thin film. Other SEM images (not shown) confirm the presence of nanocrystals on and in the polyamide film. Morphological differences reflect structural differences (i.e., extents of cross-linking) that result from changing conditions during the interfacial polymerization reaction and heat curing steps.[6]

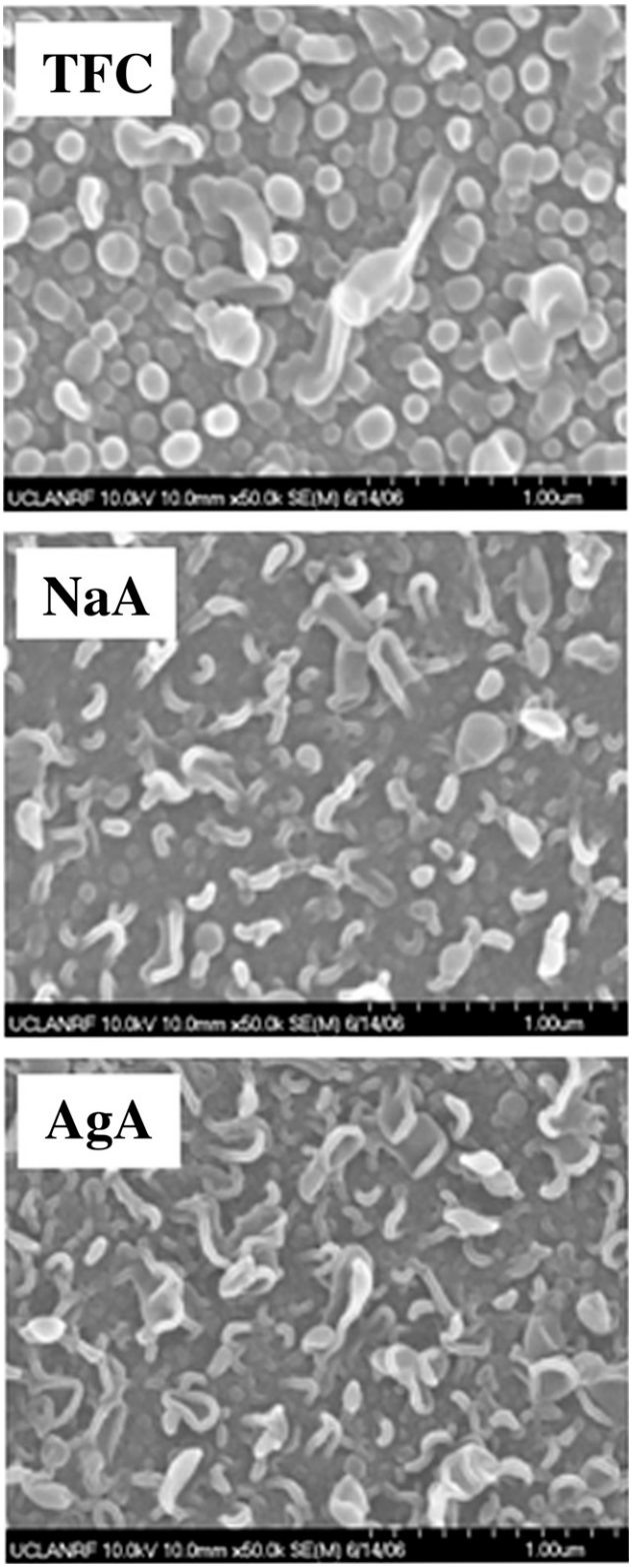

FIG. 5. SEM images of TFC, NaA-TFN, and AgA-TFN membranes taken at 25,000× magnification.

In Fig. 6 few bacteria cells deposited on the surface of NaA-TFN membranes, but TFC membranes experience significant accumulation of bacteria cells—about 3% to 5%. Although only the fractional surface coverage on the

TFC is small, within 1 h bacterial microcolonies can form on the TFC membrane, which will ultimately lead to biofilm formation and membrane fouling. In a practical water treatment application, this will lead to formation of a biofilm and severe membrane fouling over longer operating times. The duration of these tests is short, so the result may not translate directly into observable fouling resistance in a full-scale RO plant. However, TFN membranes appeared inherently more resistant to initial bacterial adhesion, which might slow down the early stages of microcolony formation, and ultimately, biofilm formation and biofouling in a practical RO process.

It is widely known that pure silver has antimicrobial properties.[19,20] For example, McDonnell et al.[21] investigated the antimicrobial properties of AgA zeolite coating films. Stainless steel plates were coated with contiguous, micron-thick coatings of NaA and AgA crystals. The authors observed significant antimicrobial activity over several days of AgA coated samples, whereas bacterial proliferated on both uncoated and NaA coated steel plates.

Here, bacterial inactivation tests were performed on as-synthesized TFC membranes, TFC membranes surface modified by depositing NaA and AgA nanocrystals on their surfaces, and TFN membranes prepared with NaA and AgA nanocrystals. The key difference between modified-TFC membranes and TFN membranes is that zeolite nanocrystals are embedded within the thin films of TFN membranes, but resting on top of the thin films for modified-TFC membranes. Representative fluorescence microscopy images are presented in Fig. 7.

Bright green dots represent live *P. putida* cells, whereas red dots represent dead cells. A significant amount of background green fluorescence comes from the polyamide material itself, which is excited by the wavelength of green fluorescence used. More than 90% of bacteria cells in the original stock solution were viable. The AgA nanoparticles produce substantial bacterial inactivation, as seen from the large number of red dots and clusters on TFC membranes modified by AgA nanoparticles. The antimicrobial activity of AgA nanocrystals was largely eliminated when the particles were embedded within the polymer film. Although a few dead cells are visible on the AgA-TFN membranes, it is unclear if they were inactivated directly by the nanocrystals or simply dead cells deposited from the bulk.

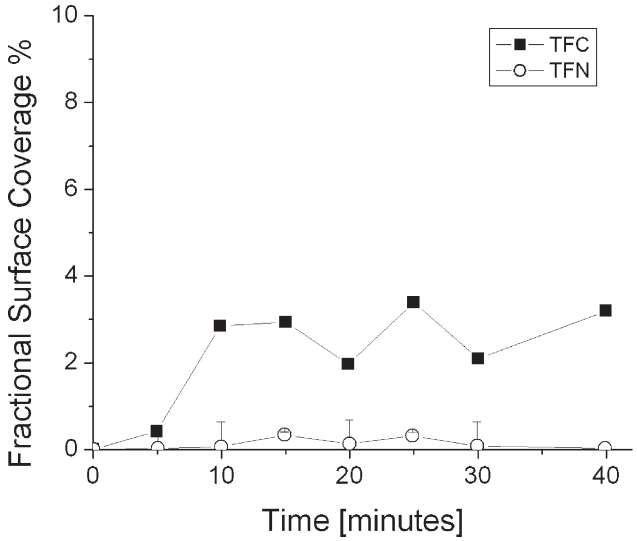

FIG. 6. Plot of bacterial adhesion on TFC and NaA-TFN membranes. Cells were deposited with no permeation through the membrane at a cross-flow Reynolds number of ~200. Feed suspension contained 10-mM NaCl and 4.2×10^6 *P. putida* cells per mL at unadjusted pH of 5.8 ± 0.2 and temperature of 20 ± 2 °C.

IV. DISCUSSION

The TFN membranes made with NaA and AgA nanocrystals have dramatically increased pure water fluxes over the base TFC membrane. This has significant

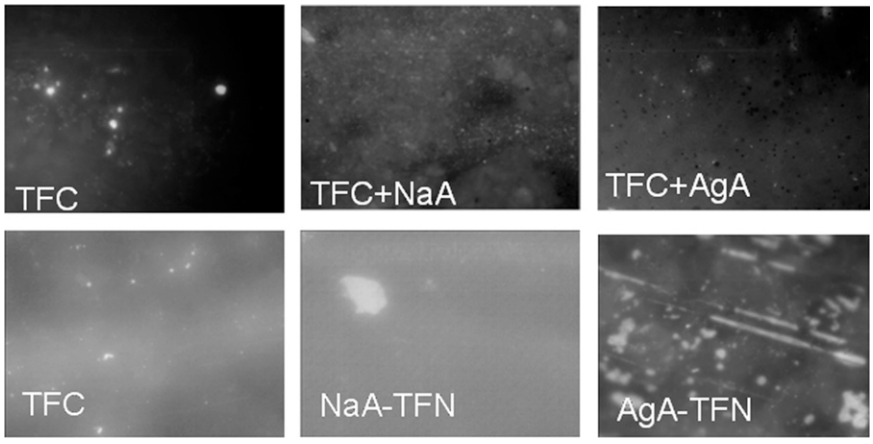

FIG. 7. Fluorescence microscope images of bacteria cells deposited onto hand-cast membranes. The cells were stained with fluorescent molecular probes. The top row shows a bare TFC membrane (left), TFC membranes surface modified with NaA (middle), and AgA (right) nanocrystals. The bottom row shows TFC (left), NaA-TFN (middle), and AgA-TFN (right) membranes. Live cells are seen on all membranes, dead cells are seen in the upper left corner of TFC+AgA.

implications for energy savings if nanocomposite RO membranes can be fabricated into commercial scale RO membrane modules. The AgA-TFN membrane exhibits ~60% increase in flux over the TFC membrane. In a wastewater reclamation application, for example, the membrane accounts for about 50% of the total energy consumption. Hence, a TFN membrane could produce about 30% more water than an equivalent TFC membrane with the same energy consumption. Alternatively, a TFN membrane could produce the same amount of water as the TFC membrane while consuming 30% less energy.

Recently, Gosh et al.[6] systematically studied factors influencing the interfacial polymerization of polyamide thin films for TFC membranes, including temperature of the organic phase. The interfacial polymerization reaction is fundamentally diffusion limited because of the high reactivity of the amine and acid chloride monomers. However, the reaction is exothermic, therefore input of heat reduces MPD-TMC reactivity while simultaneously increasing MPD diffusivity in the organic phase. Membranes formed at higher temperature exhibit higher permeability, greater cross-linking, and "leafy" surface features, whereas membranes formed at a lower temperature were less permeable, cross-linked, and had small nodular surface features.

We suspect the heat of hydration of the different LTA nanocrystals altered interfacial polymerization kinetics and the resulting thin film structure and morphology. Ostomel et al.[22] measured the heats of hydration for LTA and various cation-exchanged LTA zeolite nanocrystals. Apparently, LTA zeolites have very high heats of hydration (ranging from 640 $J \cdot g^{-1}$ for NaA to 420 $J \cdot g^{-1}$ for AgA) and hydration capacity. The hydration process creates local temperatures as large as 95 °C for NaA-type particles and 38 °C for AgA particles. During the interfacial polymerization reaction, when the TMC reacts with MPD there are opportunities for LTA nanocrystals to hydrate and release heat. Higher local temperatures may increase MPD diffusivity and reduce MPD-TMC reactivity, which changes the rates of nucleation and growth of polymer chains and the ultimate cross-linked network structure.

The effect of nanocrystals on thin film morphology is clear in the SEM images (Fig. 5). The TFC membrane exhibits nodulelike surface morphology, whereas the NaA and AgA membranes have leafier, lobelike protuberances. The density of surface features is higher in the TFC membrane and the polymer strands appear most densely packed; they appear less densely packed in the AgA membrane and the least densely packed in the NaA membrane. This decreased packing of polymer strands in the NaA membrane, formed with nanocrystals producing the greatest heat of hydration, further supports the idea that the kinetics of polymerization change in the presence of LTA nanocrystals.

It is common to use x-ray photoelectron spectroscopy (XPS) to elucidate the extent of cross-linking in polyamide thin films; however, oxygen from LTA nanocrystals produces artificially low N/O ratios, which prevents quantitative interpretation of the extent of cross-linking of nanocomposite polyamide films.[23,24] However, using the apparent correlation of surface morphology with cross-linking established by Gosh et al.,[6] we can infer the impacts of nanocrystals during the polymerization reaction. The leafier, lobelike morphologies and higher water flux of the TFN membranes made with NaA nanoparticles and AgA nanoparticles suggest they are thinner, but more cross-linked than the normal TFC membrane. These observations indirectly support the hypothesis that nanocrystals release heat as they become hydrated during the interfacial polymerization reaction. Localized temperature increases in the reaction zone may locally decrease thickness and increase cross-linking of the polyamide film.

Finally, the purple-brown color of the AgA-TFN film (Fig. 2) suggests that insoluble silver species formed during the interfacial polymerization reaction. SLS is present in the aqueous monomer solution used in the polymerization reaction. At 0.02% SLS, there is ~200 $mg \cdot l^{-1}$ of free sodium in the aqueous monomer solution. It is difficult to quantify the actual volume of aqueous solution present in the PSf support after treatment by the air knife, but the available sodium ions might exchange with some silver ions as the AgA nanocrystals enter the reaction zone. Additionally, when the amide bond forms during the polymerization reaction both hydrogen and chloride ions are released into the reaction zone. The zeolites might scavenge some hydrogen ions simply by reaction with surface silanol groups, which are almost completely dissociated at the pH (~8–9) of the aqueous monomer solution. Furthermore, hydrogen ions could exchange for silver ions within the crystals. Another possibility is that released silver ions react directly with sulfate groups of SLS.

Any combination of these potential mechanisms for silver release and precipitation during interfacial polymerization could account for the lack of antimicrobial activity exhibited by AgA-TFN membranes. Moreover, given the rather low areal density of zeolites nanocrystals exposed at the interface of the polyamide films, there are few opportunities for deposited bacteria to interact with AgA nanocrystals. Future research will focus on increasing AgA nanoparticle incorporation while retaining exchanged silver ions, which may prove valuable because biological fouling is a major performance limitation and cost factor for practical RO processes.[25]

V. CONCLUSIONS

The addition of laboratory synthesized LTA zeolite nanocrystals to polyamide thin films produced RO membranes with improved separation performance, interfacial

properties, and fouling resistance. The higher water permeability of TFN membranes is partially attributed to the super-hydrophilic zeolite molecular sieves providing a preferential flow path for water through the cross section of the thin films. However, analysis of TFC and TFN membrane morphology combined with what is known for interfacial polymerization of MPD and TMC suggests LTA nanocrystals alter the interfacial polymerization kinetics and polyamide thin film structure. In addition, silver-exchanged LTA zeolites produced membranes with higher flux and rejection, plus smoother and more hydrophilic interfaces than those formed from as-synthesized LTA in the sodium form. The strong antimicrobial reactivity of silver-exchanged LTA nanocrystals demonstrated here suggests the possibility of developing more fouling resistant membrane materials. However, more research is needed to optimize AgA nanoparticle incorporation into polyamide thin films in addition to controlling the release of silver ions during the interfacial polymerization process.

ACKNOWLEDGMENTS

The authors acknowledge financial support provided by the UCLA California NanoSystems Institute and $NanoH_2O$, Inc. We are also grateful to Prof. Bruce Dunn at UCLA for providing access to the ATR-IR instrument, Prof. Chi-Ming Ho at UCLA for providing access to the AFM instrument, and Prof. Sharon Walker's lab at UC Riverside for providing access to the streaming potential analyzer. E.M.V. Hoek and B-H. Jeong have financial interest in one of the project sponsors, $NanoH_2O$, Inc. through stock ownership and consulting agreements.

REFERENCES

1. M. Elimelech: The global challenge for adequate and safe water. *J. Water Supply Res Technol. Aqua* **55,** 3 (2006).
2. N. Savage and M.S. Diallo: Nanomaterials and water purification: Opportunities and challenges. *J. Nanopart. Res.* **7,** 331 (2005).
3. E.M.V. Hoek and A.K. Ghosh: *Nanotechnology-based Membranes for Water Purification, Nanotechnology Applications: Solutions for Improving Water Quality* (Elsevier, Atlanta, GA, 2008).
4. H.S. Lee, S.J. Im, J.H. Kim, H.J. Kim, J.P. Kim, and B.R. Min: Polyamide thin-film nanofiltration membranes containing TiO_2 nanoparticles. *Desalination* **219,** 48 (2008).
5. B.H. Jeong, E.M.V. Hoek, Y.S. Yan, A. Subramani, X.F. Huang, G. Hurwitz, A.K. Ghosh, and A. Jawor: Interfacial polymerization of thin film nanocomposites: A new concept for reverse osmosis membranes. *J. Membr. Sci.* **294,** 1 (2007).
6. A.K. Ghosh, B.H. Jeong, X.F. Huang, and E.M.V. Hoek: Impacts of reaction and curing conditions on polyamide composite reverse osmosis membrane properties. *J. Membr. Sci.* **311,** 34 (2008).
7. E.M. Vrijenhoek, S. Hong, and M. Elimelech: Influence of membrane surface properties on initial rate of colloidal fouling of reverse osmosis and nanofiltration membranes. *J. Membr. Sci.* **188,** 115 (2001).
8. S. Wang, G. Guillen, and E.M.V. Hoek: Direct observation of microbial adhesion to mermbranes. *Environ. Sci. Technol.* **39,** 6461 (2005).
9. A. Subramani and E.M.V. Hoek: Direct observation of initial microbial deposition onto reverse osmosis and nanofiltration membranes. *J. Membr. Sci.* **319,** 111 (2008).
10. S.T. Kang, A. Subramani, E.M.V. Hoek, M.A. Deshusses, and M.R. Matsumoto: Direct observation of biofouling in cross-flow microfiltration: Mechanisms of deposition and release. *J. Membr. Sci.* **244,** 151 (2004).
11. M. Pasmore, P. Todd, S. Smith, D. Baker, J. Silverstein, D. Coons, and C.N. Bowman: Effects of ultrafiltration membrane surface properties on Pseudomonas aeruginosa biofilm initiation for the purpose of reducing biofouling. *J. Membr. Sci.* **194,** 15 (2001).
12. Y. Li, T.S. Chung, and S. Kulprathipanja: Novel Ag^+-zeolite/polymer mixed matrix membranes with a high CO_2/CH_4 selectivity. *AIChE J.* **53,** 610 (2007).
13. S. Kim and E.M.V. Hoek: Interactions controlling biopolymer fouling of reverse osmosis membranes. *Desalination* **202,** 333 (2007).
14. P.S. Singh, S.V. Joshi, J.J. Trivedi, C.V. Devmurari, A.P. Rao, and P.K. Ghosh: Probing the structural variations of thin film composite RO membranes obtained by coating polyamide over polysulfone membranes of different pore dimensions. *J. Membr. Sci.* **278,** 19 (2006).
15. A.P. Rao, S.V. Joshi, J.J. Trivedi, C.V. Devmurari, and V.J. Shah: Structure-performance correlation of polyamide thin film composite membranes: Effect of coating conditions on film formation. *J. Membr. Sci.* **211,** 13 (2003).
16. M.W. Urban: *Vibrational Spectroscopy of Molecules and Macromolecules on Surfaces* (John Wiley & Sons, Inc., New York, 1993).
17. T. Kyotani, N. Shimotsuma, and S. Kakui: FTIR-ATR study of the surface of a tubular zeolite NaA membrane ultrasonically reacted with water and acetic acid. *Anal. Sci.* **22,** 325 (2006).
18. S. Alfaro, C. Rodriguez, M.A. Valenzuela, and P. Bosch: Aging time effect on the synthesis of small crystal LTA zeolites in the absence of organic template. *Mater. Lett.* **61,** 4655 (2007).
19. G.J. Zhao and S.E. Stevens: Multiple parameters for the comprehensive evaluation of the susceptibility of Escherichia coli to the silver ion. *Biometals* **11,** 27 (1998).
20. I. Sondi and B. Salopek-Sondi: Silver nanoparticles as antimicrobial agent: A case study on E. coli as a model for gram-negative bacteria. *J. Colloid Interface Sci.* **275,** 177 (2004).
21. A.M.P. McDonnell, D. Beving, A.J. Wang, W. Chen, and Y.S. Yan: Hydrophilic and antimicrobial zeolite coatings for gravity-independent water separation. *Adv. Funct. Mater.* **15,** 336 (2005).
22. T.A. Ostomel, P.K. Stoimenov, P.A. Holden, H.B. Alam, and G.D. Stucky: Host-guest composites for induced hemostasis and therapeutic healing in traumatic injuries. *J. Thromb. Thrombolysis* **22,** 55 (2006).
23. S.Y. Kwak, S.H. Kim, and S.S. Kim: Hybrid organic/inorganic reverse osmosis (RO) membrane for bactericidal anti-fouling. 1. Preparation and characterization of TiO_2 nanoparticle self-assembled aromatic polyamide thin-film-composite (TFC) membrane. *Environ. Sci. Technol.* **35,** 2388 (2001).
24. C.Y.Y. Tang, Y.N. Kwon, and J.O. Leckie: Probing the nano- and micro-scales of reverse osmosis membranes: A comprehensive characterization of physiochemical properties of uncoated and coated membranes by XPS, TEM, ATR-IR, and streaming potential measurements. *J. Membr. Sci.* **287,** 146 (2007).
25. H.C. Flemming, G. Schaule, T. Griebe, J. Schmitt, and A. Tamachkiarowa: Biofouling: The Achilles heel of membrane processes. *Desalination* **113,** 215 (1997).